ADVANCED MATERIALS
www.advmat.de

Open-Source Throttling of CD8$^+$ T Cells in Brain with Low-Intensity Focused Ultrasound-Guided Sequential Delivery of CXCL10, IL-2, and aPD-L1 for Glioblastoma Immunotherapy

Lei Dong, Yini Zhu, Haoge Zhang, Lin Gao, Zhiqi Zhang, Xiaoxuan Xu, Leqian Ying, Lu Zhang, Yue Li, Zhengcheng Yun, Danqi Zhu, Chang Han, Tingting Xu, Hui Yang, Shenghong Ju, Xiaoyuan Chen,* Haijun Zhang,* and Jinbing Xie**

Improving clinical immunotherapy for glioblastoma (GBM) relies on addressing the immunosuppressive tumor microenvironment (TME). Enhancing CD8$^+$ T cell infiltration and preventing its exhaustion holds promise for effective GBM immunotherapy. Here, a low-intensity focused ultrasound (LIFU)-guided sequential delivery strategy is developed to enhance CD8$^+$ T cells infiltration and activity in the GBM region. The sequential delivery of CXC chemokine ligand 10 (CXCL10) to recruit CD8$^+$ T cells and interleukin-2 (IL-2) to reduce their exhaustion is termed an "open-source throttling" strategy. Consequently, up to 3.39-fold of CD8$^+$ T cells are observed with LIFU-guided sequential delivery of CXCL10, IL-2, and anti-programmed cell death 1 ligand 1 (aPD-L1), compared to the free aPD-L1 group. The immune checkpoint inhibitors (ICIs) therapeutic efficacy is substantially enhanced by the reversed immunosuppressive TME due to the expansion of CD8$^+$ T cells, resulting in the elimination of tumor, prolonged survival time, and long-term immune memory establishment in orthotopic GBM mice. Overall, LIFU-guided sequential cytokine and ICIs delivery offers an "open-source throttling" strategy of CD8$^+$ T cells, which may present a promising strategy for brain-tumor immunotherapy.

1. Introduction

Despite continuous breakthroughs in surgery, chemotherapy, and radiation therapy, glioblastoma (GBM) continues to face great clinical difficulties, with poor patient prognosis and high recurrence rates.[1,2] Immunotherapy has attracted widespread attention as a promising therapeutic strategy for a wide range of tumors.[3] For example, anti-PD-1/PD-L1 antibodies (e.g., Nivolumab and Pembrolizumab) have been approved to treat advanced non-small cell lung cancer (NSCLC).[4,5] Interleukin-2 (IL-2) and anti-cytotoxic T lymphocyte-associated antigen-4 (CTLA-4) antibodies have shown significant survival benefits in the treatment of metastatic renal cell carcinoma (RCC).[6]

However, inflammatory cytokines and immune checkpoint inhibitors have not shown significant therapeutic effects in clinical trials of GBM.[5] This is mainly due to the significantly suppressive TME with T-cell exhaustion, as the number of CD8$^+$ T-cells is extremely low and the remaining CD4$^+$ T-cells function as regulatory T-cells (T_{reg}) exhibiting an unresponsive status to antigen stimulation.[5,6] Reversing the immunosuppressive TME by improving the quantity and function of T cells is a promising while challenging immunotherapy strategy against GBM.[7] CXC chemokine ligand 10 (CXCL10) can effectively

L. Dong, L. Ying, L. Zhang, Z. Yun, T. Xu, H. Zhang
Nurturing Center of Jiangsu Province for State Laboratory of AI Imaging & Interventional Radiology; Department of Oncology
Zhongda Hospital
Medical School
Southeast University
87 Dingjiaqiao, Nanjing 210009, China
E-mail: haijunzhang@seu.edu.cn

Y. Zhu
Department of Microbiology and Immunology
Medical School of Southeast University
Nanjing, Jiangsu 210009, China

H. Zhang, L. Gao, Z. Zhang, X. Xu, D. Zhu, C. Han, S. Ju, X. Chen, J. Xie
Nurturing Center of Jiangsu Province for State Laboratory of AI Imaging & Interventional Radiology
Basic Medicine Research and Innovation Center of Ministry of Education
State Key Laboratory of Digital Medical Engineering
Department of Radiology
Zhongda Hospital
Medical School of Southeast University
Nanjing 210009, China
E-mail: jsh@seu.edu.cn; xiejb@seu.edu.cn

Y. Li
State Key Laboratory of Quality Research in Chinese Medicine
Institute of Chinese Medical Sciences
University of Macau
Macau SAR 999078, China

The ORCID identification number(s) for the author(s) of this article can be found under https://doi.org/10.1002/adma.202407235

DOI: 10.1002/adma.202407235

recruit immune cells, especially T cells, and promote their migration and adhesion to tumor tissues.[7] Interleukin-2 (IL-2) reduces $CD8^+$ T cell exhaustion (T_{ex}) and enhances their immunomodulatory effects, paving the way for a more potent and sustained immune response.[6,8] Cytokines are subject to rapid clearance and metabolism in the body, resulting in a narrow therapeutic window during circulation.[5,6,9] Consequently, the short half-life of cytokine in vivo, the narrow therapeutic window during circulation, the high rate of failure in clinical trials, and the high occurrence of serious adverse events are notable concerns.[6,8,9]

Moreover, the brain-tumor-barrier (BTB), which separates brain-tumor tissue from macromolecular drugs in circulating blood, leading to insufficient penetration of macromolecular drugs into the brain, thus limiting the efficacy of cytokine and antibody in GBM treatment.[10,11] Recent studies have shown that materials such as polymer scaffolds, hydrogels, and nanoparticles have been explored for the transport of macromolecular drugs such as cytokines or antibodies.[12,13] However, tumor tissues are heterogeneous, including high pressure, dense cellular arrangement, and abnormal vascular structure.[10,12] These factors can limit the diffusion and penetration of nanocarriers in tumor tissues, making drug delivery compromised.[12] Therefore, overcoming BTB for deep tumor delivery remains a great challenge for brain tumor therapy.[12,13]

Low-intensity focused ultrasound (LIFU) combined with microbubbles (MBs) enhances anti-GBM immunotherapy by opening the BTB, shows promise for delivering free antibodies and cytokines to brain tumors.[14–16] However, excess circulating antibodies or cytokines may lead to potential tissue and organ toxicity concerns.[17–19] In order to concentrate immunotherapeutic agents in GBM while reducing systemic exposure, scientists tried to develop drug-loading MBs and nanobubbles to simultaneously open BTB and delivery immunotherapeutic drugs.[20–24] However, whether drug-loading influences on MBs' characteristics or size influences on nano bubbles would bring challenges on their cavitation effects.[20,21,25]

Based on these facts, we designed a strategy for LIFU-guided sequential delivery of cytokines and immune checkpoint inhibitors (ICIs) without affecting the "cavitation effect" of MBs. Under exposure of LIFU at 0.40 w cm^{-2}, the CXCL10-loaded phospholipid microbubbles (C@MBs) were triggered to open BTB and release CXCL10 into GBM to recruit $CD8^+$ T cells. Under exposure of LIFU at 1.58 w cm^{-2}, the mature DC cell membranes (DM) fusing with PLGA loading IL-2 and aPD-L1 (IP@DCNBs) were triggered the release of IL-2 for reducing $CD8^+$ T cells exhaustion, and aPD-L1 for enhancing $CD8^+$ T cells activity (**Figure 1**). This strategy enhances the infiltration of $CD8^+$ T cells in the GBM region and reduces the exhaustion of $CD8^+$ T cells, which significantly improves the immunotherapeutic efficacy. It is named"open-source throttling" effect on $CD8^+$ T cells.[6,7,26]

2. Results

2.1. Prognosis of GBM Patients is Related to the Ability of $CD8^+$ T Cells

We performed data mining of the TCGA and GTEx databases using the online platform http://gepia2.cancer-pku.cn/. High $CD8^+$ T cell exhaustion-related gene expression was linked to poor patient prognosis, while high expression of Treg cell-related genes was negatively associated with prognosis. Additionally, increased PD-L1 expression in GBM hindered immune response and protected tumor cells from $CD8^+$ T cell-mediated killing (Figure S1, Supporting Information). These results suggest that the therapeutics aimed at increasing the number of $CD8^+$ T cells and reversing their exhaustion status within TME represent a promising strategy for treating GBM.

2.2. Characterization of C@MBs and IP@DCNBs

C@MBs loaded with CXCL10, which functions to recruit $CD8^+$ T cells (**Figure 2a**). Atomic force microscopy and optical microscopy images demonstrated well-dispersed C@MBs with consistent morphology (Figures 2b and S2a,b, Supporting Information). The particle size measurement revealed an average diameter of 1178 nm and an average zeta potential of 16 mV for the C@MBs (Figures 2d and S2b, Supporting Information). Additionally, the stability of C@MBs was evaluated over 7 days in PBS (pH 7.4), DMEM or 10% FBS, revealing negligible changes in particle size and concentration (Figures 2e and S2b,c, Supporting Information). The encapsulation efficiency of CXCL10 was determined to be 96% with a drug loading capacity of 1.3% using a zymography method (Table S1, Supporting Information). As the acoustic intensity of LIFU action increased, the concentration of the C@MBs suspension decreased, leading to a reduction in both particle size and surface charge (Figures 2f,g and S2d, Supporting Information).

Mature DC 2.4 cell membranes (DM) were fused with PLGA to form DCNBs targeting GBM with a "cavitation effect".[21,24,27]

H. Yang
Department of Biochemistry and Molecular Biology
Medical School of Southeast University
Nanjing, China

X. Chen
Departments of Diagnostic Radiology, Surgery, Chemical and Biomolecular Engineering, and Biomedical Engineering
Yong Loo Lin School of Medicine and College of Design and Engineering
National University of Singapore
Singapore 119074, Singapore
E-mail: chen.shawn@nus.edu.sg

X. Chen
Nanomedicine Translational Research Program
NUS Center for Nanomedicine
Yong Loo Lin School of Medicine
National University of Singapore
Singapore 117597, Singapore

X. Chen
Clinical Imaging Research Centre
Centre for Translational Medicine
Yong Loo Lin School of Medicine
National University of Singapore
Singapore 117599, Singapore

X. Chen
Institute of Molecular and Cell Biology
Agency for Science
Technology, and Research (A*STAR)
61 Biopolis Drive, Proteos, Singapore 138673, Singapore

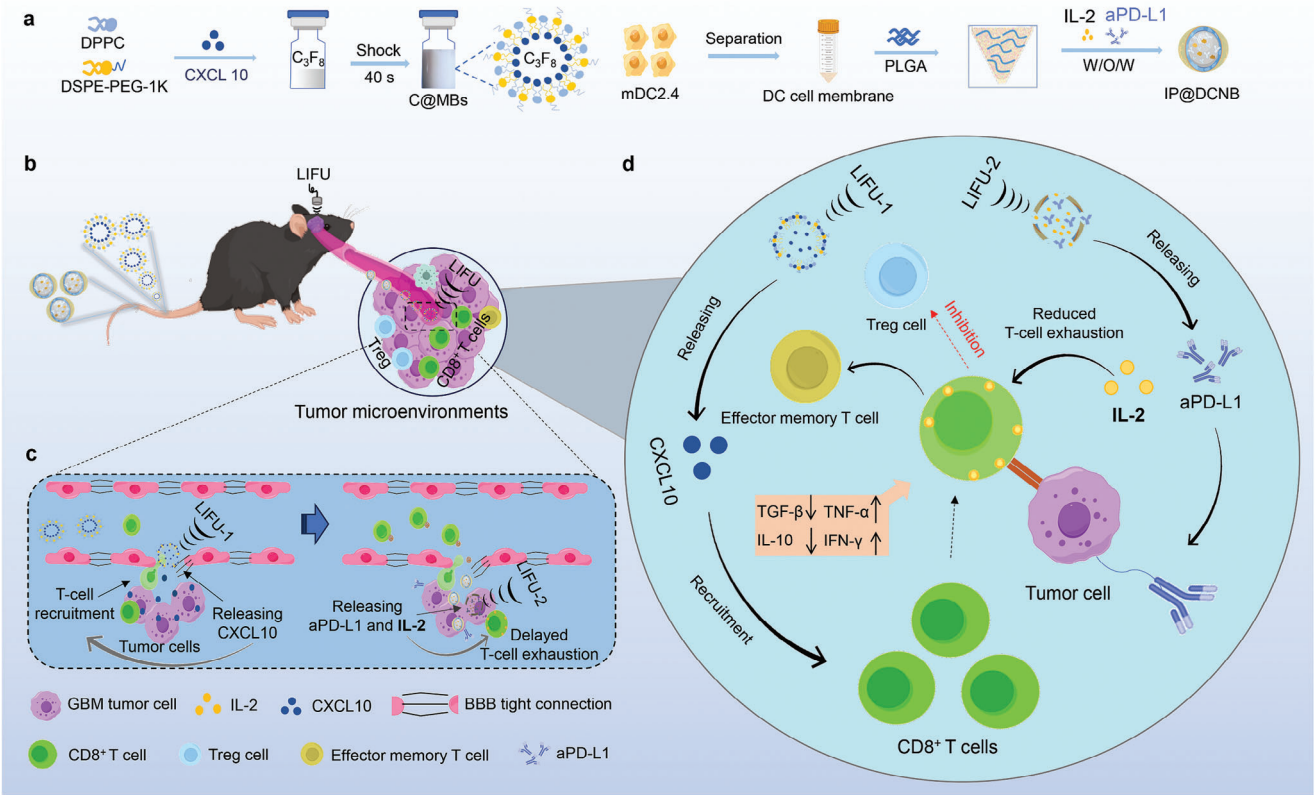

Figure 1. A LIFU-guided "open-source throttling" strategy on $CD8^+$ T cells to enhance GBM immunotherapy (By Figdraw). a) Construction model of C@MBs and IP@DCNBs. b) Therapeutic strategy for GBM in situ mouse model. c) LIFU in combination with C@MBs opens BBB and BTB and releases CXCL10 to the GBM region, LIFU in combination with IP@DCNBs releases IL-2 and aPD-L1 to the GBM region. d) Specific mechanism of "open-source throttling" strategy targeting $CD8^+$ T cells.

IL-2 and aPD-L1 were encapsulated via W/O/W re-emulsion into IP@DCNBs, creating bionic nanobubbles (Figure 2h). Immunofluorescence detection confirmed the transformation of immature DC cells (imDC) into mDCs, exhibiting high expression of CD80 and CD86 molecules (Figure S3, Supporting Information). IP@DCNBs demonstrated superior biocompatibility compared to IP@NBs, attributed to the specific binding of DM to GBM cells (Figure S4, Supporting Information). Scanning electron microscopy (SEM) images revealed well-dispersed and morphologically uniform IP@DCNBs, while transmission electron microscopy (TEM) images displayed their essential hollow structure for the "cavitation effect" (Figure 2i,j). The hybridization of PLGA with mDC cell membranes resulted in reduced shell stiffness and enhanced "cavitation" of IP@DCNBs. Dynamic light scattering (DLS) measurements showed an average diameter of 327 nm and an average zeta potential of −41 mV for IP@DCNBs (Figures 2k and S5a, Supporting Information). aPD-L1 and IL-2 were encapsulated with high efficiency (62% and 95%, respectively), resulting in drug loadings of 7.5% and 0.09%, respectively (Figure 2l,m; Table S1, Supporting Information). Additionally, the stability of IP@DCNBs was evaluated over 7 days in PBS (pH 7.4), DMEM, or 10% FBS, revealing negligible changes in particle size and concentration (Figures 2n and S5b,c, Supporting Information). The "cavitation" effect of IP@DCNBs under LIFU was verified by examining changes in particle size at different acoustic intensities. At an ultrasonic intensity of 1.58 w cm^{-2}, the post-"cavitation" particle size was reduced to 96 nm (Figure S6, Supporting Information).

2.3. Releasing of CXCL10 to Recruit T-Cells

LIFU with a sound intensity of 0.40 w cm^{-2} triggered the release of CXCL10 from C@MBs, as observed by the presence of CXCL10 in the lower chamber of the transwell by zymography quantification and *IVIS* (Figure S7a–c, Supporting Information). The number recruited T cells from the upper compartment to the lower chamber of a transwell was assessed using flow cytometry and CCK-8 assays, as shown in **Figure 3**a. Compared to the PBS-treated group, the free CXCL10 or LIFU-C@MBs group exhibited a significant increase in T cell recruitment to the lower chamber (Figures 3b,d and S7d,e, Supporting Information). Furthermore, the treatment with LIFU-C@MBs did not impact the recruitment effect of CXCL10 on T cells, and none of the three treatments affected T cell viability in the lower chamber (Figure 3c). Moreover, the blood-brain barrier (BBB) in vivo could be successfully opened when LIFU-C@MBs with ultrasonic intensity ranging from 0.40 to 2.81 w cm^{-2} was administered for 60 s, and the extent of the open area increased with higher sound intensities (Figure S8a, Supporting Information). LIFU-C@MBs

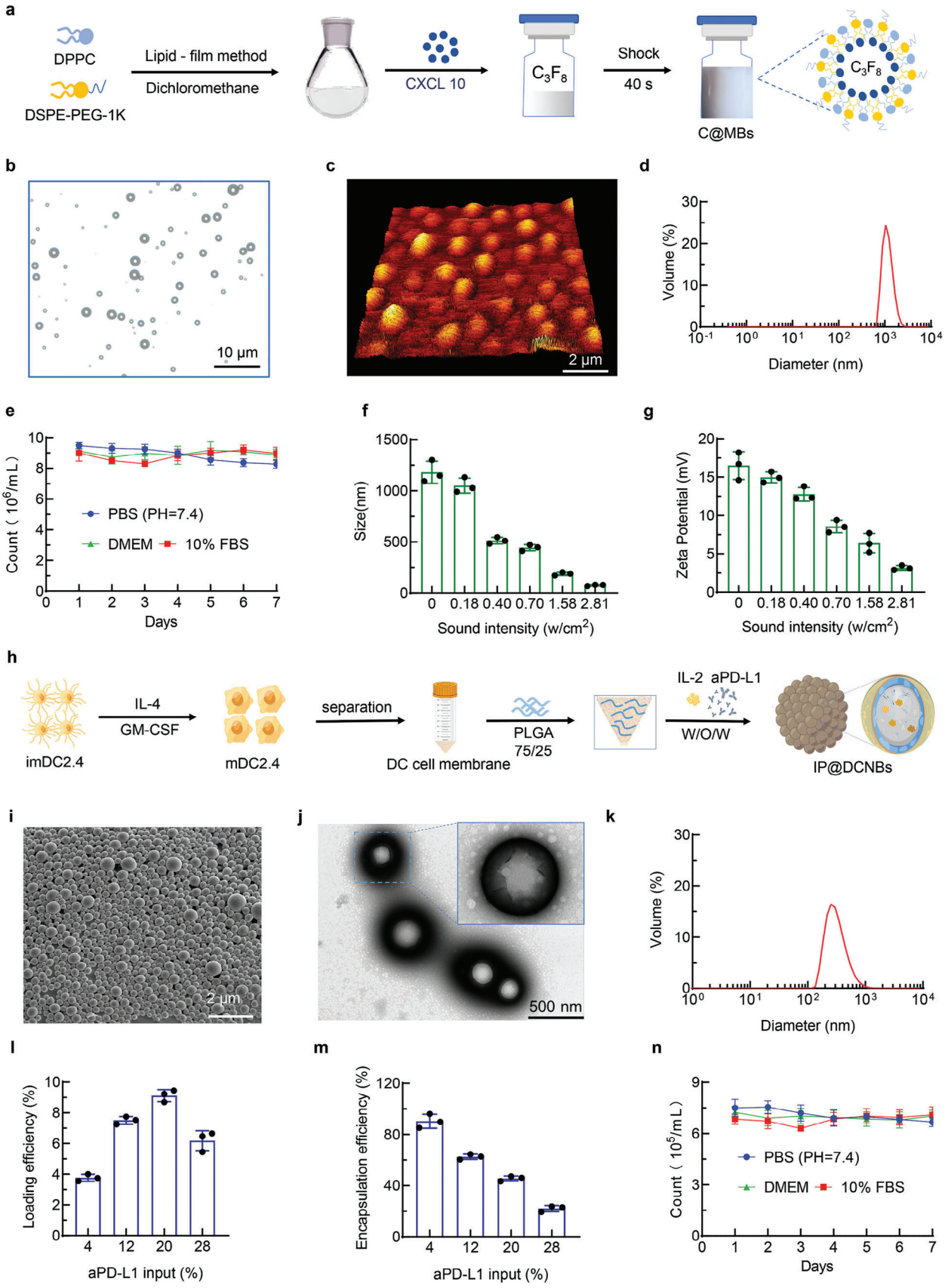

increased the content of CXCL10 in brain tissue positively with the ultrasound intensity (Figure S8b, Supporting Information). However, neither LIFU alone nor LIFU combined with IP@DCNBs could effectively open the BBB (Figure S8a, Supporting Information). The size and depth of the BBB opening region were evaluated by observing the penetration of EB dye in frozen sections (Figure 3e) when using LIFU-incorporated C@MBs. It was further observed that the BBB opening induced by LIFU combined with C@MBs was reversible, with the optimal opening effect lasting for ≈3 h and gradual recovery occurring within 6 h (Figure S9, Supporting Information). Therefore, LIFU combined with C@MBs can safely and reversibly open the BBB, effectively avoiding the trauma and risk of infection associated with traditional surgery and injections.

Compared to free CXCL10, the combination of LIFU with C@MBs resulted in a remarkable 46-fold increase in CXCL10 levels within the brain tissue, an effect that could not be achieved by C@MBs treatment alone (Figures 3f,g and S10a,b, Supporting Information). Meanwhile, LIFU combined with C@MBs reduced the residual CXCL10 in peripheral tissues and organs (Figure S10c,d, Supporting Information). Additionally, flow cytometry analysis revealed a significant increase in the proportion of both $CD8^+$ T cells and $CD4^+$ T cells in total lymphocytes recruited into the BBB-opening region when LIFU was combined with C@MBs, as compared to the other groups (Figures 3h,I and S10e,f, Supporting Information). Flow cytometry analysis showed a 1.72-fold increase in the proportion of tumor antigen-specific $CD3^+CD8^+$ T cells and a 2.69-fold increase in the proportion of IFN-γ^+CD8^+ T cells in the brain tumor region, compared with free CXCL10 (Figure S11a–d, Supporting Information). Free CXCL10 treatment did not increase tumor-specific T cell proportions in the GBM region compared to the control group. This was due to CXCL10 entering the GBM region in minimal amounts and being quickly metabolized in circulation. These results indicated that LIFU combined with C@MBs not only led to an increase in the number of $CD8^+$ T cells in the GBM region but also enhanced their antitumor performance.

2.4. In Vitro and In Vivo Biosafety

Furthermore, we conducted a biosafety assessment of LIFU and the diverse materials employed in this investigation. CCK-8 assay demonstrated that each constituent exerted a negligible impact on the viability of PC12 cells (Figure S12, Supporting Information). To further evaluate the in vivo stability and ultrasound imaging ability of the microbubbles, C@MBs, and IP@DCNBs were observed to be stable in vivo for over 30 min under CEUS and B-Mode mode monitoring of a Mindray-ZS3 small animal ultrasound imaging system (Figure S13, Supporting Information). In addition, significant in situ ultrasound imaging of GBM in C@MBs was observed in the contrast-enhanced mode of ultrasound compared to Sonovue, whereas IP@DCNBs were relatively poorly imaged (Figure S14, Supporting Information). These findings suggest that IP@DCNBs and C@MBs possess excellent dispersion, stability, ultrasound "cavitation," and imaging effects.

To assess the potential in vivo toxicity of these agents, comprehensive hematological and histological analyses were performed.[7,28] These analyses encompassed the evaluation of routine blood parameters such as red blood cells, white blood cells, platelets, and neutrophils, as well as the assessment of serum biochemical markers including alanine aminotransferase (AST), aspartate aminotransferase (ALT), total bilirubin (T-BIL), uric acid (UA), blood urea nitrogen (BUN), and creatinine (CREA). Notably, no significant changes were observed in any of the treatment groups, indicating that the combination of LIFU-C@MBs with LIFU-IP@DCNBs is biologically safe and associated with minimal side effects (Tables S2 and S3, Supporting Information). Pharmacokinetic experiments showed that C@MBs and IP@DCNBs had longer circulation times compared to free CXCL10, IL-2, or aPD-L1 (Figure S15, Supporting Information). Hematoxylin-eosin (H&E) staining of vital internal organs further revealed negligible signs of inflammation or damage (Figure S16, Supporting Information). Thus, each component utilized in the construction of the microbubbles demonstrated a favorable safety profile in vivo.

The optimal parameters for safe and reversible blood-brain barrier (BBB) opening through LIFU combined with C@MBs were further investigated using H&E staining of brain tissue sections, immunofluorescence TUNEL apoptosis assay, and inflammatory factor assay. Results showed that at sound intensities of 1.10 and 1.58 w cm^{-2}, blood cells within the BBB-opening region of brain tissue were significantly exuded, and peripheral nerve cells exhibited significant apoptosis (Figures S17 and S18, Supporting Information). Furthermore, at a sound intensity of 1.58 w cm^{-2}, inflammatory factors such as IL-10, IL-6, IL-1β, and TNF-α were significantly increased, while a sound intensity of 0.40 w cm^{-2} resulted in relatively safe BBB opening (Figures S19–S22, Supporting Information). These findings collectively indicate that the combination of LIFU with C@MBs provides a relatively safe, reversible, and efficient approach for delivering CXCL10 into the brain with a sound intensity of 0.40 w cm^{-2}.

2.5. Blockade of CD8+ T Cell Exhaustion

In our aforementioned findings, it was observed that IP@DCNBs combined with LIFU did not induce BBB opening in vivo. *IVIS* and zymography assays showed that LIFU with a sound intensity of 1.58 w cm^{-2} triggered the release of aPD-L1 from IP@DCNBs

Figure 2. Characterization of C@MBs, IP@DCNBs. a) Schematic structure of C@MBs. b) Optical microscope image of C@MBs. c) Atomic force microscopy (AFM) images of C@MBs. d) The average particle size of C@MBs was 1178.7 ± 97.29 nm. e) Concentration changes of C@MBs resuspended in PBS (pH 7.4), DMEM, or 10% FBS was continuously monitored for 7 days (n = 3). f,g) Changes in particle size potential of C@MBs after 60 s of different acoustic intensities (n = 3). h) Schematic structure of IP@DCNBs. i,j) Scanning electron microscope (SEM) and transmission electron microscope (TEM) images of IP@DCNBs. k) The average particle size of IP@DCNBs was 327.32 ± 11.83 nm. l,m) The loading and encapsulation rates of IP@DCNBs correspond to different input ratios of aPD-L1 (n = 3). n) Concentration changes of IP@DCNBs resuspended in PBS (pH 7.4), DMEM, or 10% FBS was continuously monitored for 7 days (n = 3). All statistics are expressed as mean ± standard deviation. Statistical significance was calculated by one-way ANOVA with the Tukey post hoc test.

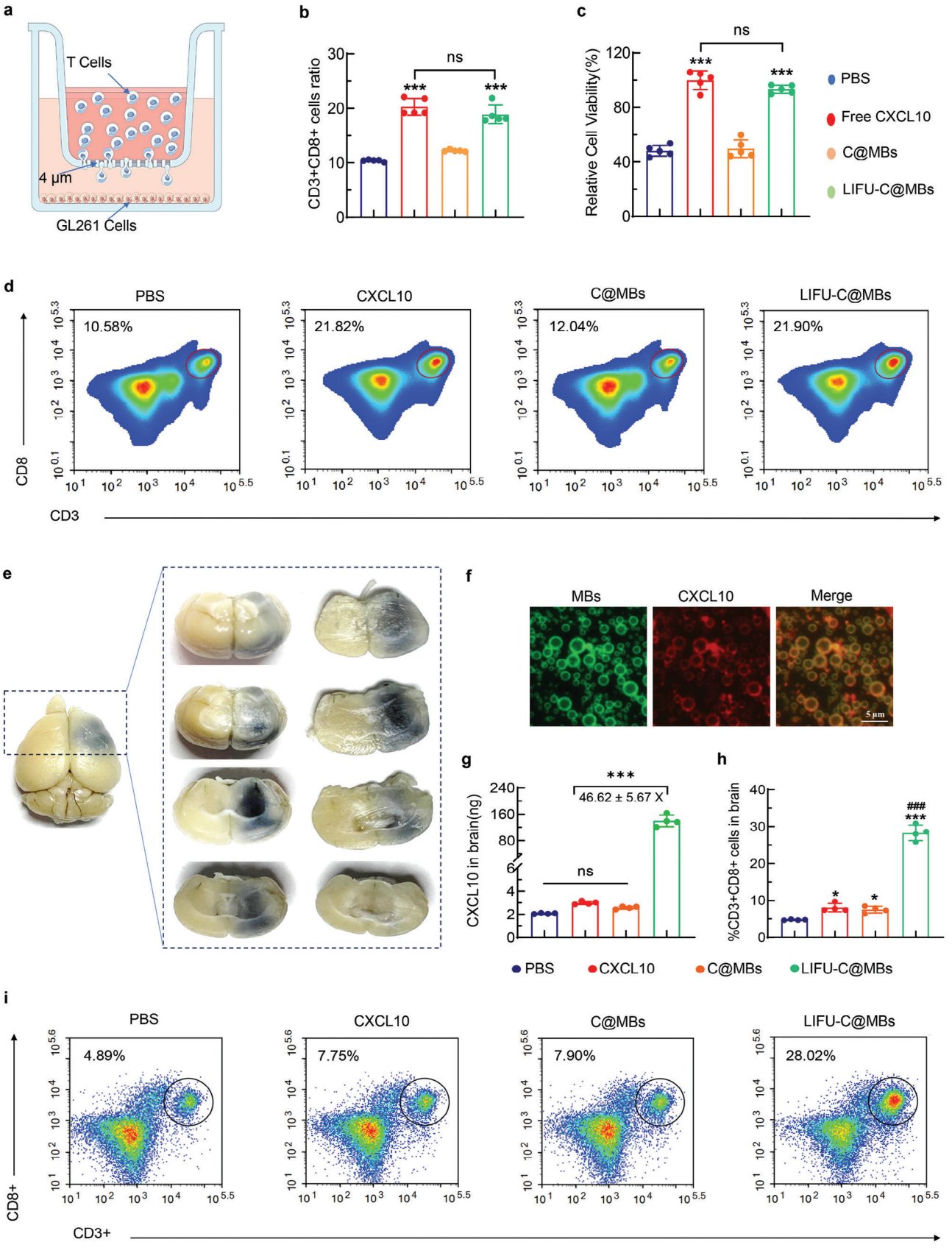

(Figure S7f–h, Supporting Information). To delve deeper into its "cavitation effect", an in vitro BTB model was constructed using bEnd.3 cells (Figure S23a, Supporting Information). The effect on blocking T cell exhaustion was further evaluated via LIFU binding to IP@DCNBs (**Figure 4a**). Quantitative fluorescence analysis by zymography revealed that the combination of LIFU and IP@DCNBs effectively opened the BTB model and facilitated the release of IL-2 and aPD-L1 into the lower compartment (Figure S23b,c,f, Supporting Information). In addition, flow assay results showed that the number of CTLL-2 cells in the LIFU combined with IP@DCNBs treatment group was 8.34-fold higher than that in the IL-2-only treatment group (treated on chamber) (Figure S23d,e,g, Supporting Information). Moreover, the CCK-8 assay indicated a substantial 4.97-fold increase in CTLL-2 cell viability and a notable 6.44-fold decrease in GL261 cell viability in the LIFU combined with IP@DCNBs-treated group, as compared to the PBS-treated group (Figure S24a,b,d, Supporting Information). And a 72 h prolongation of CTLL-2 cellular activity following direct IL-2 addition to the lower compartment or LIFU combined with IP@DCNBs treatment, compared to the untreated control group (Figure S24c, Supporting Information).

Furthermore, we conducted a gray value analysis of WB bands using ImageJ with flow-through analysis. This analysis revealed a significant decrease in the expression of CTLL-2 cellular exhaustion indicators, namely PD1, Tim3, and CTLA4, in the group treated with LIFU combined with IP@DCNBs (Figure 4b–f). These results indicate that the BTB can be effectively opened, and IL-2 can be released through the treatment of LIFU combined with IP@DCNBs, thereby preventing T-cell exhaustion. Importantly, these findings are consistent with the positive control (Equivalent amount of IL-2 at a concentration of 50 ng/mL added directly to the lower chamber of the transwell) results, highlighting the effective release of IL-2 via the BTB by LIFU combined with IP@DCNBs treatment, without affecting the protein activity of IL-2.

2.6. Delivery Efficiency of IL-2 and aPD-L1

As depicted in Figure S23 (Supporting Information), at an ultrasound intensity of 1.58 w cm^{-2}, IP@DCNBs caused the disassembly of ZO-1 tight junction proteins in the BTB model under the influence of LIFU. Moreover, LIFU in combination with IP@DCNBs treatment resulted in a significant increase in the content of aPD-L1 in the lower compartment compared to IP@DCNBs treatment alone. Furthermore, the content of IL-2-cy5 in brain tissue was quantified using enzyme labeling, and the results demonstrated a 17.68-fold increase in IL-2 after applying LIFU with a sound intensity of 0.40 w cm^{-2} combined with C@MBs for 60 s (Figure S25a, Supporting Information). Subsequently, the delivery efficiency of LIFU in conjunction with IP@DCNBs was further examined in the GL261 in situ GBM mouse model. *IVIS* results demonstrated that LIFU combined with IP@DCNBs led to elevated deep brain tissue aPD-L1 content, with the reduced distribution of aPD-L1 in organs such as the liver and kidney (Figure 4g–j). Notably, fluorescence microscopy revealed that LIFU in combination with IP@DCNBs significantly augmented aPD-L1 content in the GBM region (Figure S25b,c, Supporting Information). Additionally, the IP@DCNBs-treated group exhibited a marked increase in aPD-L1 content in brain tissues compared to the aPD-L1 group, owing to the presence of mDC cell membrane components targeting GBM in the shells of IP@DCNBs.

2.7. The Effects on Orthotopic Glioma Mouse Model

To further evaluate the in vivo anti-tumor effect, a dual fluorescein in situ GBM mouse model was constructed (Figures S26–S28, Supporting Information). The proportion of the tumor relative to the entire brain volume was measured every 5 days using MRI to track the progression of the tumor (**Figure 5a**).

As shown in Figures 5b,d and S29 (Supporting Information), mice treated with PBS, free aPD-L1 and free IP exhibited tumor progression, indicating that systemic delivery of IL-2 and aPD-L1 failed to achieve effective T-cell responses and tumor elimination. However, tumor growth was significantly inhibited, and survival was significantly prolonged with the treatment of LIFU-C@MBs combined with LIFU-IP@DCNBs (Figure 5c). On the other hand, mice that received free IP therapy had a short survival time of <37 days and significant weight loss (Figure S30a, Supporting Information). The results of histological analysis of brain tumor tissues (including tumor proliferation reflected by PCNA with Ki-67 staining and tumor cell apoptosis reflected by TUNEL staining on day 20 post-treatment) showed that tumor proliferation was significantly inhibited and tumor cell apoptosis was significantly increased in the LIFU-C@MBs combined with LIFU-IP@DCNBs-treated group of mice compared to the other groups (Figures 5e–g and S30b, Supporting Information). The above experimental findings were indirectly verified by the results of the in vivo imaging system (*IVIS*) assay (Figure S31, Supporting Information).

2.8. The Anti-Tumor Capacity of CD8+ T Cells in GBM was Improved

To elucidate the activation process, changes in inflammatory cytokines within tumors were quantified via ELISA after different

Figure 3. LIFU triggers C@MBs to release CXCL10 to recruit T cells. a) Schematic representation of the experimental procedure of the ex vivo T cell chemotaxis assay for demonstrating the chemotactic effect of LIFU-directed CXCL10 release from C@MBs on T cells. b–d) Quantification of the proportion of $CD8^+$ T cells in total cells in the lower compartment by flow cytometry after treatment with different CXCL10 preparations for 3 h ($n = 5$). Relative cell viability of lower compartment T cells after treatment with different CXCL10 preparations was determined by CCK-8 assay ($n = 5$). e–g) Observation of the penetration of Evan's blue dye (20 µL of 2% EB/only) to assess the effect of LIFU in combination with C@MBs to open the BBB; Dio-labeled MBs, Cy5-labeled CXCL10, multifunctional enzyme markers quantification of CXCL10 in brain tissue (LIFU corresponding to a sound intensity of 0.4 w cm^{-2}, $n = 4$). h,i) Flow quantification of the proportion of recruited $CD8^+$ T cells after opening the BBB by LIFU (0.40 w cm^{-2}) combined with C@MBs ($n = 4$). Data are expressed as mean ± standard deviation. Statistical significance was calculated by one-way ANOVA with the Tukey post hoc test. $^{*}p < 0.05$, $^{**}p < 0.01$, $^{***}p < 0.001$, and $^{\#\#\#}p < 0.001$, ns: no significance.

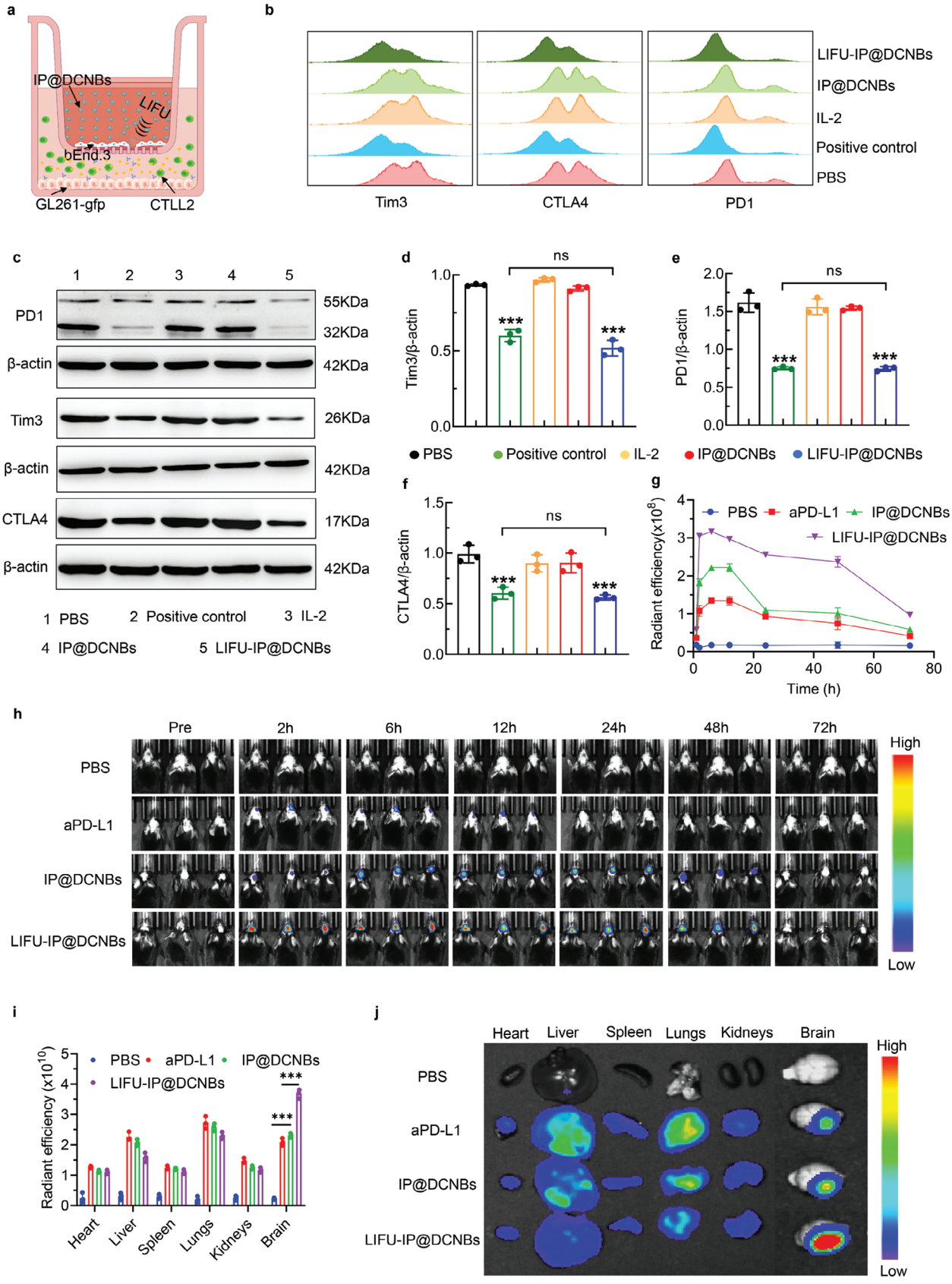

treatments. The findings depicted in **Figure 6**a–e demonstrate that the administration of LIFU-C@MBs combined with LIFU-IP@DCNBs rapidly increased the levels of pro-inflammatory factors TNF-α and IFN-γ, while diminished anti-inflammatory factors TGF-β and IL-10 in GBM. This confirms the impact of LIFU-C@MBs combined with LIFU-IP@DCNBs on modulating the immune microenvironment. Furthermore, following a series of treatments of LIFU-C@MBs combined with LIFU-IP@DCNBs, intra-tumor levels of TNF-α and IFN-γ were significantly upregulated, exhibiting a 7.54-fold and 3.65-fold increase, respectively, compared to mice treated with PBS. Additionally, intratumor levels of TGF-β and IL-10 were reduced by 60% and 72%, respectively. This phenomenon suggests that accurately delivering CXCL10, IL-2, and aPD-L1 can effectively enhance the immune response against GBM, swiftly alleviating the immunosuppressive environment.

The immune cell profiles in the brains of GL261-loaded mice were further analyzed using immunofluorescence and flow cytometry techniques (Figure S32, Supporting Information). Immunofluorescent staining of GBM tumors from untreated homozygous mice showed minimal infiltration of $CD3^+CD8^+$ T cells. However, significant upregulation of the ratio of total $CD8^+$ T cells to effector $CD45^+$ T cells was observed after treatment with LIFU-C@MBs combined with LIFU-IP@DCNBs. These findings were consistent with the flow cytometry analysis, which revealed a 3.39-fold increase in the proportion of $CD3^+CD8^+$ T cells in GBM tumors compared to the *i.v.* aPD-L1 groups (Figures 6f,h and S33–S35, Supporting Information).

Moreover, the proportion of Treg cells in the LIFU-C@MBs combined with LIFU-IP@DCNBs-treated group was significantly lower compared to the free aPD-L1 group, showing a 6.82-fold decrease. Additionally, the ratio of $CD8^+$ T cells to T_{reg} cells in the LIFU-C@MBs combined with LIFU-IP@DCNBs group exhibited an 18.74-fold increase compared to the free aPD-L1 group (Figures 6g,i and S36 and S37, Supporting Information).

The expression of PD1, Tim3, and CTLA4, which are indicators of T-cell exhaustion, decreased by 4.41-fold, 3.27-fold, and 2.42-fold, respectively, in GBM tumors of the LIFU-C@MBs combined with LIFU-IP@DCNBs-treated group compared to the free aPD-L1-treated group (Figures 6j–m and S38–S41, Supporting Information). These results indicated that the treatment with LIFU-C@MBs combined with LIFU-IP@DCNBs significantly increased the number of $CD8^+$ T lymphocytes and delayed their exhaustion in GBM tumors. This effectively reversed immunosuppressive TME and enhanced the anti-tumor immune response.

Furthermore, in comparison to the free aPD-L1-treated group, the proportion of $CD62L^-CD44^+$ effector memory T cell (T_{EM}) subpopulation in the spleens of treated mice was significantly increased by 2.14-fold. Additionally, the ratio of T_{EM} to $CD62L^+CD44^+$ central memory T cells (T_{CM}) was substantially elevated by 12.94-fold (Figure S42, Supporting Information). These findings highlight the ability of LIFU-C@MBs combined with LIFU-IP@DCNBs to promote the generation and expansion of immune memory.

2.9. LIFU-C@MBs Combined with LIFU-IP@DCNBs Treatment Elicited a Prolonged immune memory

Additionally, given the notable antitumor effects witnessed in the in situ GL261 GBM model, we further investigated the preventive efficacy of sequentially delivering CXCL10, IL-2, and aPD-L1 to augment immunotherapy-induced tumor regeneration inhibition. Subsequent analysis involved assessing memory T cells in the spleens of mice that survived 45 days post-initial administration, and re-implanting tumor cells into five surviving mice for re-priming studies (Figure S43a, Supporting Information). GBM mice treated with the combination of LIFU-C@MBs and LIFU-IP@DCNBs showed minimal tumor growth upon re-implantation of GL261 compared to Naïve mice (Figure S43b,c, Supporting Information). Additionally, this treatment significantly extended the survival of mice compared to Naïve mice (Figure S43d, Supporting Information). In addition, the ratios of T_{EM}, T_{EM} to T_{CM} were significantly higher in LIFU-C@MBs combined with LIFU-IP@DCNBs-treated mice compared with Naïve mice (Figure S43e–g, Supporting Information). These results suggest that LIFU-guided sequential delivery of CXCL10, IL-2, and aPD-L1 mobilizes blood-derived T cells to effectively activate immune responses in brain tumors, which not only prolongs the effective anti-tumor activity of T cells but also triggers a long-lasting systemic immune memory to prevent tumor recurrence.[29,30]

3. Discussion

In this study, an "open-source throttling" approach has been devised for $CD8^+$ T cells to augment immunotherapy for GBM. This strategy involves the use of LIFU-guided delivery of CXCL10 to attract $CD8^+$ T cells, IL-2 to mitigate their exhaustion, and aPD-L1 to bolster the recognition and destruction of tumors.[6–9,20,26] In the clinical setting, GBM patients often do not experience significant benefits from immunotherapy due to constraints in antibody delivery and an immune microenvironment that hinders efficacy.[1,5] Despite the increased permeability caused by disruption of the BTB, this barrier retains crucial characteristics that limit the penetration of large molecule anticancer drugs into the GBM.[14,15] Additionally, the efficacy of immunotherapy in the immunosuppressive microenvironment of GBM is significantly impacted by $CD8^+$ T-cell exhaustion.[7,31] Recent research conducted in both preclinical and clinical settings has demonstrated

Figure 4. LIFU combined with IP@DCNBs to deliver IL-2 and aPD-L1. a) Schematic of the experimental procedures of IL-2 and aPD-L1 delivery for demonstrating the effect of LIFU-directed IL-2 released from IP@DCNBs on T cell exhaustion. b) Quantification of T cell expression of PD1, Tim3 and CTLA4 protein levels by flow-through ($n = 3$). c–f) Quantification of T cell expression of PD1, Tim3, and CTLA4 protein levels by WB, ImageJ analysis of strip gray values ($n = 3$). g,h) Fluorescence quantification of changes in the content of Cy5-labeled aPD-L1 in the brain at different time points after incapacitation ($n = 3$). i,j) Fluorescence quantification of heart, liver, spleen, lungs, kidneys, brain, and other organs distribution of Cy5-labeled aPD-L1 after incapacitation and other organs distribution. Data are expressed as mean ± standard deviation. Statistical significance was calculated by one-way ANOVA with the Tukey post hoc test. $^{***}p < 0.001$, ns: no significance.

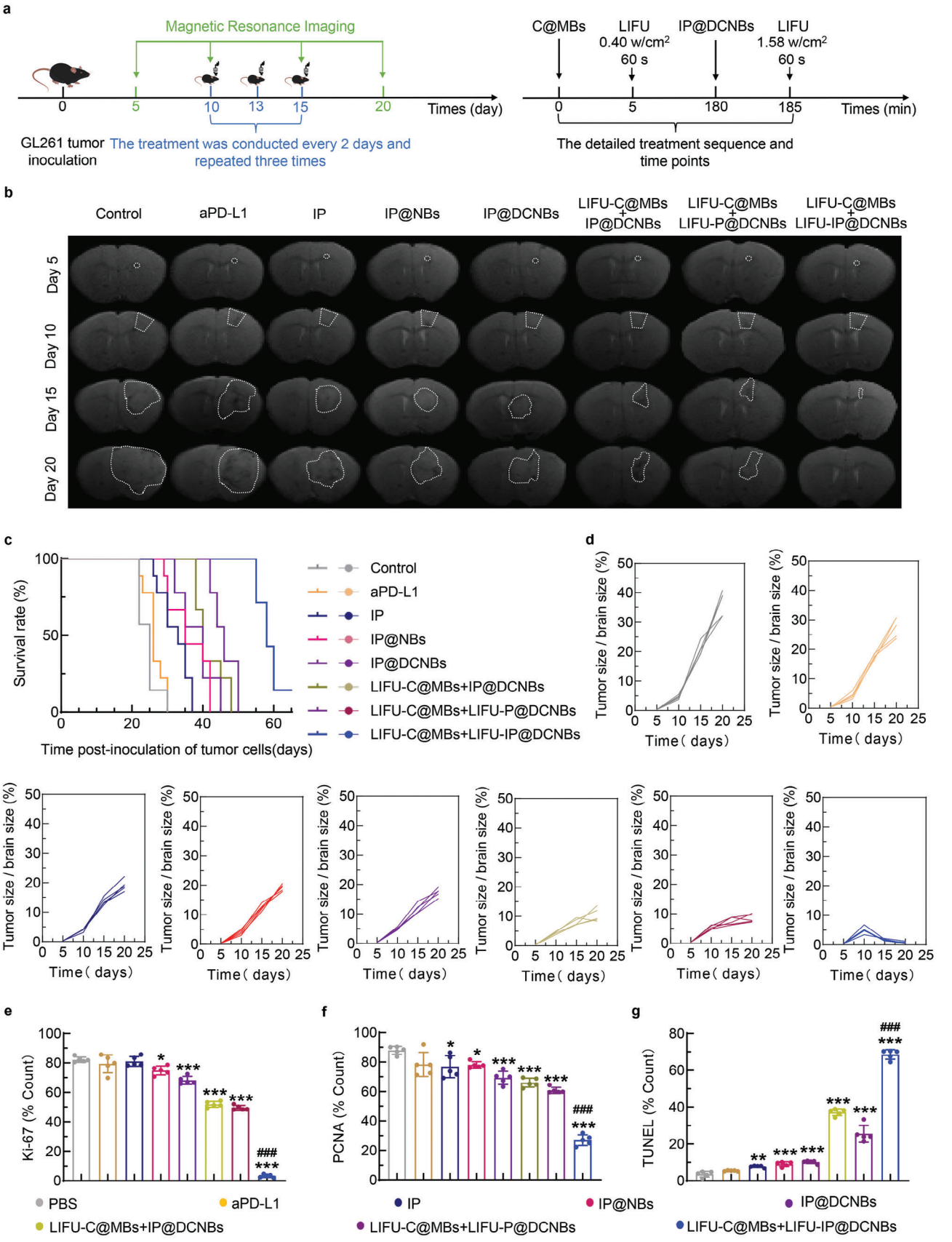

that ultrasound microbubble-targeted disruption technology can greatly enhance the efficiency of BBB permeation.[14,15]

In comparison to planar ultrasound, the combination of LIFU with MBs provides the benefit of precise drug delivery to specific regions of the brain.[25,26] LIFU operates at levels that avoid tissue damage, offering precise targeting, particularly at the BBB/BTB.[21,22] MBs, injected intravenously, range from a few to tens of micrometers in diameter.[25] When exposed to ultrasound, MBs oscillate within blood vessels, exerting localized physical effects.[25,26] This interaction enhances BBB permeability by creating localized pressure and shear forces, facilitating the passage of therapeutic substances into brain tissue.[21,25] LIFU combined with MBs is typically non-invasive, avoiding surgical risks associated with craniotomy and reducing recovery times.[21,25] This approach's ability to precisely control ultrasound focus and energy, alongside the safety profile of microbubbles, ensures clinical feasibility and safety.[25,32] The approval granted by the US Food and Drug Administration (FDA) for the use of focused ultrasound in the treatment of conditions such as uterine fibroids, bone metastases, breast cancer, prostate cancer, and liver tumors highlights the diverse potential applications of this technology in medical treatment.[28,32–34]

Recent studies have shown that LIFU/MBs enhances the accumulation of immune adjuvants in brain TME and improves survival in different mouse brain tumor models, including GBM.[21,22,32] But there are still many challenges. For example, large amounts of antibodies or cytokines remain in the circulation, which is bound to cause tissue and organ toxicity.[19,35,36] Further refinement of the design of "immune-enhancing MBs" to enhance the content of immune adjuvants in the localized region of MBs has become a key research direction in this field.[14,36,37] MBs' low drug loading capacity restricts efficacy.[37] PLGA nanobubbles have high drug loading capacity but poor ability to undergo "cavitation" to improve BTB penetration efficiency (Figure S8a, Supporting Information).[14,20,23,24,38,39] These cases may limit the maximization of the immunotherapeutic effect of LIFU/MBs to enhance GBM.[20,32,39]

In this study, we used LIFU-guided sequential delivery of cytokines and antibodies to the localized region of GBM to overcome the above problems. The results showed that LIFU/C@MBs could effectively open to increase the penetration of BBB/BTB, resulting in a 46-fold elevation of CXCL10 content in the localized region of GBM, compared with free CXCL10 (Figure 3g). Meanwhile, the opening of BBB/BTB by LIFU/C@MBs also increased the delivery of IP@DCNBs in the GBM.[14,36,39,40] The shell layer of IP@DCNBs consists of a fusion of PLGA and DM, which not only enhances its ability to undergo the "cavitation effect", but also facilitates the antigen-presentation process of T cells.[14,23,24,37,41] Therefore, compared with the conventional method of single-factor delivery, our study not only represents a technological breakthrough but also offers significant advantages in terms of improving therapeutic efficacy and minimizing side effects.[14,37] This strategy further strengthens the concept of LIFU-guided spatial tumor-targeted (local-regional) brain cancer immunotherapy and provides an important theoretical and practical basis for future immunotherapy development.[36,42]

GBM, a challenging "cold tumor," features diminished $CD8^+$ T cell numbers and function, limiting current immunotherapy effectiveness.[1,2,35,43] Immunoregulatory factors like Treg cells and suppressive cytokines (e.g., TGF-β, IL-10) exacerbate $CD8^+$ T cell exhaustion and hinder their tumor infiltration.[35,44–48] $CD8^+$ T cells are crucial for tumor elimination; chemokines recruit them effectively, and IL-2 enhances their function and persistence.[6,8,30] Combining LIFU with microbubbles significantly boosted CXCL10 (46-fold) and IL-2 (17-fold) delivery to GBM regions.[21] Immunofluorescence and flow cytometry confirmed increased $CD8^+$ T cell infiltration and reduced Treg cell proportions in tumors, validating this approach's efficacy.[3,5] Additionally, it enhances large molecule drug delivery and tumor response to aPD-L1, reversing GBM's immunosuppression and improving immunotherapy outcomes.[4,5] It also promotes effector memory T cells expansion in mice, establishing durable immune memory against tumor recurrence.[29,30,49]

Focused ultrasound's potential for non-invasive brain treatment of once-incurable diseases sparks significant scholarly interest, despite its inherent limitations.[25,28,33,37] The Focused Ultrasound Foundation's ongoing research has identified nearly 40 potential applications in neurology and psychiatry, many in early stages.[14,34,37] Currently, LIFU primarily treats lesions near the central nervous system.[14,50,51] Variations in skull composition limit LIFU candidacy, underscoring the need for cautious optimism about its future.[33,41] Researchers strive to overcome these hurdles, enhancing LIFU's accessibility.[22,24,33,52,53]

In summary, our studies present a strategy for enhancing the delivery of macromolecular drugs to the brain and increasing the efficacy of immunotherapy for brain tumors.[5,53] This "open-source throttling" strategy, which targets $CD8^+$ T-cells, may have broader implications for immunotherapy in treating other immunosuppressive cancers.

4. Experimental Section

GBM Mice Model and Treatments: GL261 cells or GL261-luc cells (1×10^5 cells) were intracranially inoculated on day 0. On day 10 post-inoculation, mice were randomly assigned to receive treatments via tail vein injection: aPD-L1, IL-2 & aPD-L1, IP@NBs, IP@DCNBs, LIFU-IP@DCNBs, LIFU-C@MBs + LIFU-P@DCNBs, and LIFU-C@MBs + LIFU-IP@DCNBs. The treatment involved aPD-L1 (1.5 mg kg^{-1}), CXCL10, and IL-2 (each 75 μg kg^{-1}), administered three times at 5-day intervals. For LIFU-C@MBs + LIFU-IP@DCNBs, LIFU at 0.40 w cm^{-2} ultrasound intensity was applied to the GBM region 60 s. After 3 h, IP@DCNBs were intravenously injected, followed by LIFU at 1.58 w cm^{-2} ultrasound intensity to the GBM region for 60 s.

Figure 5. Treatment efficacy on orthotopic glioma mouse model. a) Treatment schedule of the GL261 mouse brain tumor model. The detailed treatment sequence and time points. b) Brain images of each group of mice obtained by T2 MRI with different treatments, where tumors are circled in white dashed lines. c) Survival curves of hormonal glioma mice treated with various aPD-L1 preparations ($n = 10$). Statistical significance was calculated using the log-rank test. d) Relative tumor volumes of mice after different treatments. e-g) Immunohistochemical images of tumor sections were examined at 20 days of rhabdomyolysis (Ki67, PCNA, and TUNEL, $n = 5$). Data are expressed as mean ± standard deviation. Statistical significance was calculated by one-way ANOVA with the Tukey post hoc test. Statistical analysis of overall survival time was performed using log-rank tests. $^*p < 0.05$, $^{**}p < 0.01$, $^{***}p < 0.001$, and $^{\#\#\#}p < 0.001$, ns: no significance.

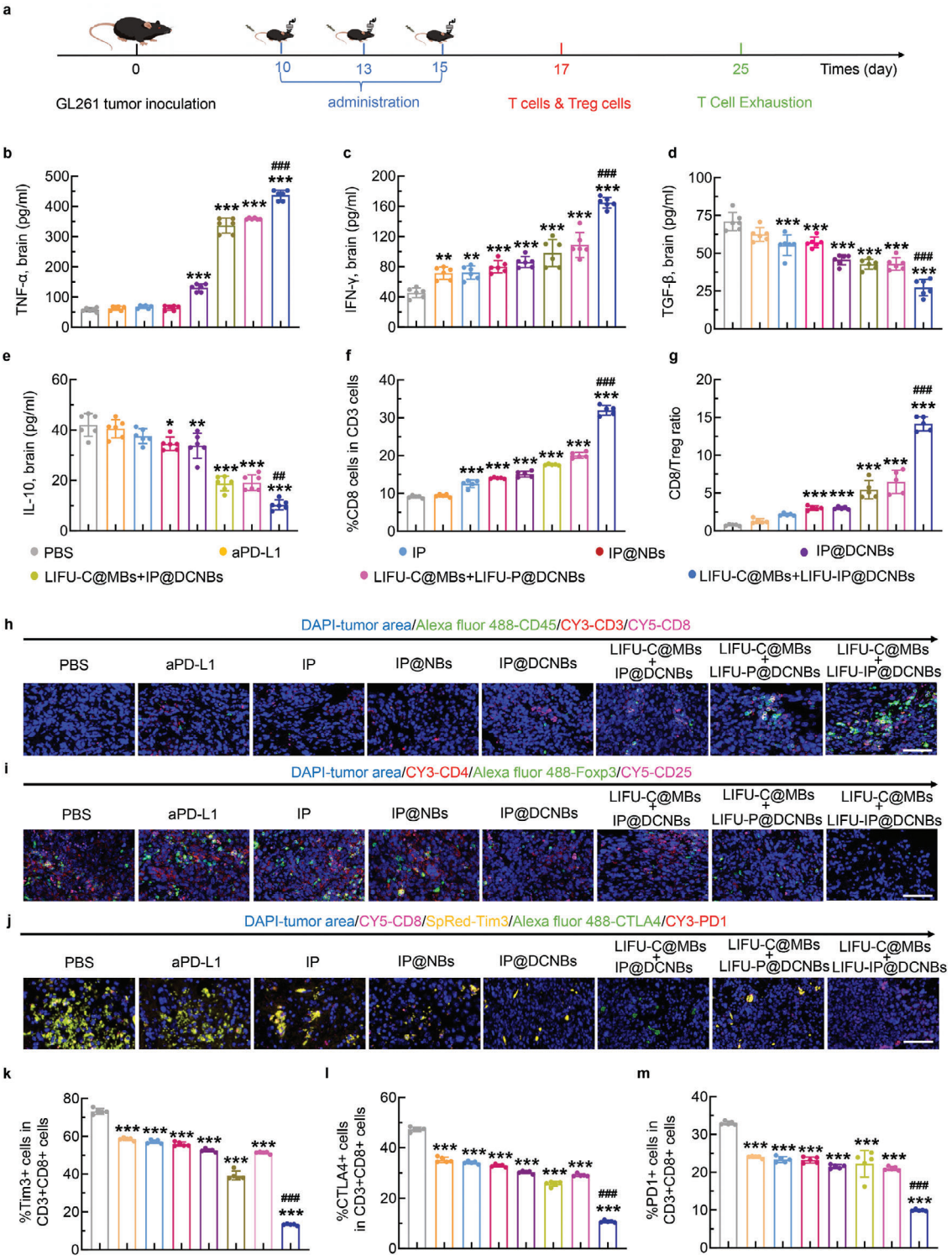

Figure 6. Efficacy of sequential delivery of CXCL10, IL-2, and aPD-L1 to reverse the immune microenvironment of glioma in situ. a) Schedule of in vivo tumor immune profiling in the GL261 mouse brain tumor model. b–e) Levels of cytokines in tumor tissues after various treatments ($n = 6$). f) Flow-type quantification of $CD45^+CD3^+$ cells in tumors as the proportion of $CD8^+$ T cells ($n = 5$). g) Tumor microenvironment activation status as determined by flow assay of the ratio of $CD8^+$ T cells to Treg cells ($n = 5$). h–j) Representative immunofluorescence images of tumor-infiltrating T cells after 72 h of different treatments (H: blue: DAPI; green: Alexa fluor 488-CD45; red: CY3-CD3; pink: Cy5-CD8; I: blue: DAPI; green: Alexa fluor 488-Foxp3; red: CY3-CD4; pink: Cy5-CD25; J: blue: DAPI; pink: Cy5-CD8; yellow: SpRed-Tim3; Green: Alexa fluor 488-CTLA4; Red: CY3-PD1; Scale bar = 50 μm). k–m) $CD8^+$ T cell exhaustion status in the tumor microenvironment was determined by flow assay of $CD8^+$ T cell expression of Tim3, CTLA4, and PD1 ratio ($n = 5$). Data are expressed as mean ± standard deviation. Statistical significance was calculated by one-way ANOVA with the Tukey post hoc test. $^{*}p < 0.05$, $^{**}p < 0.01$, $^{***}p < 0.001$, $^{\#\#}p < 0.001$, and $^{\#\#\#}p < 0.001$.

Cell Culture: Mouse cell lines CTLL-2, DC 2.4, bEnd.3, and GL261 (including GL261-luc cells with luciferase expression) were obtained from the Shanghai Institutes for Biological Sciences, Chinese Academy of Sciences. CTLL-2 cells were maintained in their specific medium, while DC 2.4, bEnd.3, GL261, and GL261-luc cells were cultured in DMEM or RPMI-1640 supplemented with 10% FBS. All cells were cryopreserved in CELL-AID serum-free solution (C40100, New Cell&Molecular Biotech, China).

Preparation and Characterization of C@MBs and IP@DCNBs: 0.125 g PLGA and 200 µg DM were dissolved in 2.5 mL CH_2Cl_2. Separately, 5 mg aPD-L1 and 150 µg IL-2 were dissolved in 0.375 mL double-distilled water, then added to the CH2Cl2 solution and emulsified with ultrasonication for 2 min to form a primary emulsion. The primary emulsion (20 mL) was added to 20 mL 1% PVA solution and emulsified for 1 min to form a complex emulsion. Isopropanol (0.625 mL) was added dropwise and stirred at room temperature for 4–6 h. The emulsion was centrifuged at 12 000 rpm for 10 min, supernatant discarded, and the precipitate washed three times with double-distilled water. The washed precipitate was stored at 80 °C for 2–3 h and freeze-dried for 24 h to obtain IL-2 and aPD-L1-loaded IP@DCNBs.

14.41 mg DPPC and 7.017 mg DSPE-PEG-1000 were dissolved in 10 mL anhydrous ethanol and evaporated at 48 °C to form a white film. This film was hydrated with 8 mL double-distilled water, 1 mL propylene glycol, and 1 mL propanetriol under ultrasonic conditions at 50 °C until fully dissolved. After ultrasonic crushing (300 W, 10 min on-off cycle), the membrane was divided into 10 aliquots, vacuum-sealed, and filled with perfluoropropane gas. Each aliquot received 30 µg of CXCL10 cytokine and was shaken for 40 s to obtain the C@MBs stock solution.

Characterization of C@MBs and IP@DCNBs was evaluated by enzyme marker, Malvern particle size meter, fluorescence microscopy, atomic force microscopy and ultrasound imaging.

H&E Staining and Immunofluorescence Analysis: For H&E staining, mouse tumor tissues were fixed in 4% paraformaldehyde, dehydrated in sucrose solutions, paraffin-embedded, sectioned, and stained with hematoxylin and eosin.

Cytokine Assays: Tumor tissues were collected, homogenized, and centrifuged, with the resulting supernatant aliquoted and diluted in Elisa assay buffer as per manufacturer instructions. Tumor levels of IFN-γ, IL-10, TGF-β, and TNF-α were quantified using specific Elisa kits (MM-0182M1, MM-0176M1, MM-0689M1, MM-0132M1, Jiangsu Enzyme Immunity Industry Co., Ltd, China).

For immunofluorescence staining, mice were slaughtered and tumor tissues were removed, which were further fixed in 4% paraformaldehyde, dried using sucrose solutions, embedded with paraffin and then sliced into slides. To evaluate $CD8^+$ T cells in GBM, tumor sections were quadruple-labeled for CD8, PD1, TIM-3, and CTLA-4 (blue: DAPI; green: Alexa fluor 488-CD45; red: CY3-CD3; pink: Cy5-CD8). To evaluate exhausted T cell exhaustion in GBM, tumor sections were quadruple-labeled for CD8, PD1, TIM-3, and CTLA-4 (blue: DAPI; pink: Cy5-CD8; yellow: SpRed-Tim3; Green: Alexa fluor 488-CTLA4; Red: CY3-PD1). To evaluate Treg cells in GBM, Tumor sections were also quadruple-labeled for CD4, CD25, Foxp3, and DAPI-labeled nuclei (blue: DAPI; green: Alexa fluor 488-Foxp3; red: CY3-CD4; pink: Cy5-CD25).

Flow Cytometric Analysis: For T-cell analysis, collagenase D (0.5 µg mL^{-1}), DNase1 (0.5 µg mL^{-1} from Vazyme Biotec Co., Ltd, China; 3 µg mL^{-1} from Sigma Aldrich, USA), and a lymphocyte isolation solution (17-5442-03, GE, USA) were used to isolate brain-infiltrating immune cells. Cells were stained with antibodies against CD45, CD3, CD4, CD8a, CD25 (103112, 100203, 100537, 100707, 102015, Biolegend, USA), and Foxp3 (126403, Biolegend, USA), followed by flow cytometry to analyze CD8+ and Foxp3+ T cell populations ($2*10^4$ events analyzed). Memory T cells were stained with antibodies against CD45, CD3, CD8a, CD44 (103112, 100203, 100707, 103029, Biolegend, USA), and CD62L (104427, Biolegend, USA), followed by flow cytometry ($2*10^4$ events analyzed).

Magnetic Resonance Imaging (MRI): MRI was performed using a 7.0 T small animal MR scanner (Bruker, Germany) with T2-weighted imaging (T2WI) and fast spin-echo sequence (TR/TE 2000/50 ms, matrix 256256, FOV 2020 mm, slice thickness 1.0 mm) to monitor tumor growth. Glioma-in situ volume was measured using ImageJ (NIH, USA), calculating relative tumor volume as glioma-in situ volume divided by whole brain volume.

In Vivo Bioluminescence Imaging: Bioluminescence imaging was used to quantify tumor load in mice carrying GL261-luc. Tumor-bearing mice were injected with D-luciferin (150 mg kg^{-1} body weight, Nanjing Starleaf Biological Technology Co., China), and images were taken using an animal live imaging system (ABL X5, Tanon, China). Data were subsequently analyzed using Living Image 2.5 software (Caliper Life Sciences, USA).

Statistical Analysis: One-way analysis of variance (ANOVA) followed by Tukey's honest significant difference (HSD) post hoc test was used to evaluate the differences of $CD8^+$ T cell ratio, antibody activity, tumor volume, body weight, inflammatory cytokine level, and data in western blotting, immunostaining, and flow cytometry analysis after various treatments. The independent sample t-test was performed to analyze and compare the tumor volume in the rechallenge study and memory T cell ratio in immune memory analysis. Statistical analysis of overall survival time was performed using log-rank tests. All statistical tests were performed using SPSS software (SPSS version 19.0, SPSS Inc., USA) and data were reported as standard deviation ± mean (S. D.). The significance is expressed as $^*p < 0.05$, $^{**}p < 0.01$, $^{***}p < 0.001$ relative to control group; $^{\#}p < 0.05$, $^{\#\#}p < 0.01$, and, $^{\#\#\#}p < 0.001$ relative to all groups; ns: no significance.

Ethical Statement: Female C57BL/6 mice (6–8 weeks old) were purchased from Jiangsu Huachuang Sino Pharma Tech Co., Ltd. All animal experiments were performed in compliance with the relevant laws and approved by the Institutional Animal Care and Use Committee of Southeast University School of Medicine (NO. 20220316049).

Supporting Information

Supporting Information is available from the Wiley Online Library or from the author.

Acknowledgements

This work was supported by the National Natural Science Foundation of China (NSFC, No. 82372023, 82172010, and 82402355). The National Key Research and Development Program of China (2022YFE0116700). The SEU Innovation Capability Enhancement Plan for Doctoral Students (CXJH_SEU 24220).

Conflict of interest

The authors declare no conflict of interest.

Author Contributions

L.D. conducted the synthesis, characterization, cell studies, animal experiments, and data analysis. L.D., H.Z., L.G., D.Z., and X.X. performed the construction of an orthotopic brain tumor model. L.D., Y.Z., Z.Z., and J.X. wrote the manuscript. L.D., Y.Z., Z.Z., Z.Y., L.Y., L.Z., C.H., T.X., H.Y., and J.C. contributed to the data analysis and discussed the data. S.J., X.C., H.Z., and J.X. conceived and designed the experiments. S.J., X.C., H.Z., and J.X. supervised the entire project. L.D., Y.Z., Y.L., and J.X. revised the manuscript. We thank the Home for Researchers editorial team (www.home-for-researchers.com) for the language editing service. Thanks to Nanjing Starleaf Biological Technology Company for the technical support of microbubble preparation.

Data Availability Statement

Research data are not shared.

Keywords

CXCL10, glioblastoma, IL-2, immune checkpoint inhibitors, immunosuppressive microenvironment, low-frequency focused ultrasound, T-cell exhaustion

Received: May 21, 2024
Revised: August 14, 2024
Published online:

[1] K. D. Miller, Q. T. Ostrom, C. Kruchko, N. Patil, T. Tihan, G. Cioffi, H. E. Fuchs, K. A. Waite, A. Jemal, R. L. Siegel, J. S. Barnholtz-Sloan, *CA Cancer J. Clin.* **2021**, *71*, 381.
[2] R. Ma, M. Taphoorn, P. Plaha, *J. Neurol. Neurosurg. Psychiatry* **2021**, *92*, 1103.
[3] O. K. Dagher, R. D. Schwab, S. K. Brookens, A. D. Posey Jr, *Cell* **2023**, *186*, 1814.
[4] M. D. Hellmann, P. A. Jänne, M. Opyrchal, N. Hafez, L. E. Raez, D. I. Gabrilovich, F. Wang, J. B. Trepel, M. J. Lee, A. Yuno, S. Lee, S. Brouwer, S. Sankoh, L. Wang, D. Tamang, E. V. Schmidt, M. L. Meyers, S. S. Ramalingam, E. Shum, P. Ordentlich, *Clin. Cancer Res.* **2021**, *27*, 1019.
[5] V. A. Arrieta, C. Dmello, D. J. McGrail, D. J. Brat, C. Lee-Chang, A. B. Heimberger, D. Chand, R. Stupp, A. M. Sonabend, *J. Clin. Invest.* **2023**, *133*, 163447.
[6] A. N. Shouse, K. M. LaPorte, T. R. Malek, *Immunity* **2024**, *57*, 414.
[7] X. Xu, Z. Zhang, J. Du, Y. Xue, X. Chen, J. Zhang, X. Yang, D. Chang, J. Xie, S. Ju, *Adv. Mater.* **2023**, *35*, 2209785.
[8] V. Niederlova, O. Tsyklauri, M. Kovar, O. Stepanek, *Trends Immunol.* **2023**, *44*, 890.
[9] X. Zheng, Y. Wu, J. Bi, Y. Huang, Y. Cheng, Y. Li, Y. Wu, G. Cao, Z. Tian, *Cell. Mol. Immunol.* **2022**, *19*, 192.
[10] L. Rong, N. Li, Z. Zhang, *J. Exp. Clin. Cancer Res.* **2022**, *41*, 142.
[11] L. R. Schaff, I. K. Mellinghoff, *JAMA, J. Am. Med. Assoc.* **2023**, *329*, 574.
[12] S. Kudruk, C. M. Forsyth, M. Z. Dion, J. K. Hedlund Orbeck, J. Luo, R. S. Klein, A. H. Kim, A. B. Heimberger, C. A. Mirkin, A. H. Stegh, N. Artzi, *Proc. Natl. Acad. Sci. USA* **2024**, *121*, 2306973121.
[13] Y. Dong, J. Zhang, Y. Wang, Y. Zhang, D. Rappaport, Z. Yang, M. Han, Y. Liu, Z. Fu, X. Zhao, C. Tang, C. Shi, D. Zhang, D. Li, S. Ni, A. Li, J. Cui, T. Li, P. Sun, O. Benny, C. Zhang, K. Zhao, C. Chen, X. Jiang, *Adv. Mater.* **2024**, *36*, 2311109.
[14] C. M. Gorick, V. R. Breza, K. M. Nowak, V. Cheng, D. G. Fisher, A. C. Debski, M. R. Hoch, Z. Demir, N. M. Tran, M. R. Schwartz, N. D. Sheybani, R. J. Price, *Adv. Drug Delivery Rev.* **2022**, *191*, 114583.
[15] L. Song, X. Hou, K. F. Wong, Y. Yang, Z. Qiu, Y. Wu, S. Hou, C. Fei, J. Guo, L. Sun, *Acta Biomater* **2021**, *136*, 533.
[16] R. U. Cardenas, M. Laramee, I. Ray, N. Dahmane, M. Souweidane, B. Martin, *J. Control Release* **2023**, *362*, 755.
[17] A. J. Ozga, M. T. Chow, M. E. Lopes, R. L. Servis, M. Di Pilato, P. Dehio, J. Lian, T. R. Mempel, A. D. Luster, *Immunity* **2022**, *55*, 82.
[18] W. Yan, L. Qiu, M. Yang, A. Xu, M. Ma, Q. Yuan, X. Ma, W. Liang, X. Li, Y. Lu, *Cancer Lett.* **2023**, *567*, 216263.
[19] A. Chow, K. Perica, C. A. Klebanoff, J. D. Wolchok, *Nat. Rev. Clin. Oncol.* **2022**, *19*, 775.
[20] S. V. Morse, A. Mishra, T. G. Chan, R. T. M. de Rosales, J. J. Choi, *J. Control Release* **2022**, *341*, 605.
[21] J. Wang, Z. Li, M. Pan, M. Fiaz, Y. Hao, Y. Yan, L. Sun, F. Yan, *Adv. Drug Delivery Rev.* **2022**, *190*, 114539.
[22] D. Wang, C. Xing, Y. Liang, C. Wang, P. Zhao, X. Liang, Q. Li, L. Yuan, *Adv. Mater.* **2024**, *36*, 2310421.
[23] S. Zhu, H. Xing, P. Gordiichuk, J. Park, C. A. Mirkin, *Adv. Mater.* **2018**, *30*, 1707113.
[24] T. Li, L. Deng, M. Xu, X. Shen, C. Wu, Y. Liu, *J Control Release* **2015**, 213, e138.
[25] S. Snipstad, K. Vikedal, M. Maardalen, A. Kurbatskaya, E. Sulheim, C. L. Davies, *Adv. Drug Delivery Rev.* **2021**, *177*, 113847.
[26] E. Alphandéry, *J. Nanobiotechnol.* **2022**, *20*, 139.
[27] X. Zhang, Y. Zheng, Z. Wang, S. Huang, Y. Chen, W. Jiang, H. Zhang, M. Ding, Q. Li, X. Xiao, X. Luo, Z. Wang, H. Qi, *Biomaterials* **2014**, *35*, 5148.
[28] A. Carpentier, R. Stupp, A. M. Sonabend, H. Dufour, O. Chinot, B. Mathon, F. Ducray, J. Guyotat, N. Baize, P. Menei, J. de Groot, J. S. Weinberg, B. P. Liu, E. Guemas, C. Desseaux, C. Schmitt, G. Bouchoux, M. Canney, A. Idbaih, *Nat. Commun.* **2024**, *15*, 1650.
[29] M. Corrado, E. L. Pearce, *J. Clin. Invest.* **2022**, *132*, 148546.
[30] A. K. Molodtsov, N. Khatwani, J. L. Vella, K. A. Lewis, Y. Zhao, J. Han, D. E. Sullivan, T. G. Searles, N. K. Preiss, T. B. Shabaneh, P. Zhang, A. R. Hawkes, B. T. Malik, F. W. Kolling, E. J. Usherwood, S. L. Wong, J. D. Phillips, K. Shirai, C. V. Angeles, S. Yan, T. J. Curiel, Y. H. Huang, C. Cheng, M. J. Turk, *Immunity* **2021**, *54*, 2117.
[31] A. Bikfalvi, C. A. da Costa, T. Avril, J. V. Barnier, L. Bauchet, L. Brisson, P. F. Cartron, H. Castel, E. Chevet, H. Chneiweiss, A. Clavreul, B. Constantin, V. Coronas, T. Daubon, M. Dontenwill, F. Ducray, N. Enz-Werle, D. Figarella-Branger, I. Fournier, J. S. Frenel, M. Gabut, T. Galli, J. Gavard, G. Huberfeld, J. P. Hugnot, A. Idbaih, M. P. Junier, T. Mathivet, P. Menei, D. Meyronet, et al., *Trends Cancer* **2023**, *9*, 9.
[32] D. Zhang, X. Wang, J. Lin, Y. Xiong, H. Lu, J. Huang, X. Lou, *Ultrason. Sonochem.* **2023**, *100*, 106608.
[33] C. Brighi, E. Salimova, M. de Veer, S. Puttick, G. Egan, *J. Control Release* **2022**, *345*, 443.
[34] R. Pandiselvam, A. Y. Aydar, N. Kutlu, R. Aslam, P. Sahni, S. Mitharwal, M. Gavahian, M. Kumar, A. Raposo, S. Yoo, H. Han, A. Kothakota, *Ultrason Sonochem* **2023**, *92*, 106261.
[35] S. Kumari, R. Gupta, R. K. Ambasta, P. Kumar, *Biochim. Biophys. Acta Rev. Cancer* **2023**, *1878*, 188913.
[36] H. Lee, Y. Guo, J. L. Ross, S. Schoen Jr, F. L. Degertekin, C. Arvanitis, *Sci. Adv.* **2022**, *8*, eadd2288.
[37] C. D. Arvanitis, V. Askoxylakis, Y. Guo, M. Datta, J. Kloepper, G. B. Ferraro, M. O. Bernabeu, D. Fukumura, N. McDannold, R. K. Jain, *Proc. Natl. Acad. Sci. USA* **2018**, *115*, E8717.
[38] G. Zhang, H. R. Ye, Y. Sun, Z. Z. Guo, *ACS Sens.* **2022**, *7*, 2857.
[39] Z. Zeng, C. Zhang, S. He, J. Li, K. Pu, *Adv. Mater.* **2022**, *34*, 2203246.
[40] Y. Li, W. Chen, Y. Kang, X. Zhen, Z. Zhou, C. Liu, S. Chen, X. Huang, H. J. Liu, S. Koo, N. Kong, X. Ji, T. Xie, W. Tao, *Nat. Commun.* **2023**, *14*, 6973.
[41] E. Memari, D. Khan, R. Alkins, B. Helfield, *J. Control Release* **2024**, *367*, 283.
[42] C. T. Curley, B. P. Mead, K. Negron, N. Kim, W. J. Garrison, G. W. Miller, K. M. Kingsmore, E. A. Thim, J. Song, J. M. Munson, A. L. Klibanov, J. S. Suk, J. Hanes, R. J. Price, *Sci. Adv.* **2020**, *6*, eaay1344.
[43] G. Oliveira, C. J. Wu, *Nat. Rev. Cancer* **2023**, *23*, 295.
[44] P. Liao, W. Wang, W. Wang, I. Kryczek, X. Li, Y. Bian, A. Sell, S. Wei, S. Grove, J. K. Johnson, P. D. Kennedy, M. Gijón, Y. M. Shah, W. Zou, *Cancer Cell* **2022**, *40*, 365.
[45] M. Philip, A. Schietinger, *Nat. Rev. Immunol.* **2022**, *22*, 209.
[46] M. Reina-Campos, N. E. Scharping, A. W. Goldrath, *Nat. Rev. Immunol.* **2021**, *21*, 718.
[47] Q. Wang, Y. Qin, B. Li, *Cancer Lett.* **2023**, *559*, 216043.
[48] L. Sun, Y. Su, A. Jiao, X. Wang, B. Zhang, *Signal Transduct Target Ther* **2023**, *8*, 235.
[49] K. Okła, D. L. Farber, W. Zou, *J. Exp. Med.* **2021**, *218*, 20201605.
[50] C. Gasca-Salas, B. Fernández-Rodríguez, J. A. Pineda-Pardo, R. Rodríguez-Rojas, I. Obeso, F. Hernández-Fernández, M. Del Álamo, D. Mata, P. Guida, C. Ordás-Bandera, J. I. Montero-Roblas, R.

Martínez-Fernández, G. Foffani, I. Rachmilevitch, J. A. Obeso, *Nat. Commun.* **2021**, *12*, 779.

[51] A. Dasgupta, T. Sun, E. Rama, A. Motta, Y. Zhang, C. Power, D. Moeckel, S. M. Fletcher, M. Moosavifar, R. Barmin, C. Porte, E. M. Buhl, C. Bastard, R. M. Pallares, F. Kiessling, N. McDannold, S. Mitragotri, T. Lammers, *Adv. Mater.* **2023**, *35*, 2308150.

[52] S. Schoen Jr, M. S. Kilinc, H. Lee, Y. Guo, F. L. Degertekin, G. F. Woodworth, C. Arvanitis, *Adv. Drug Delivery Rev.* **2022**, *180*, 114043.

[53] A. Sabbagh, K. Beccaria, X. Ling, A. Marisetty, M. Ott, H. Caruso, E. Barton, L. Y. Kong, D. Fang, K. Latha, D. Y. Zhang, J. Wei, J. DeGroot, M. A. Curran, G. Rao, J. Hu, C. Desseaux, G. Bouchoux, M. Canney, A. Carpentier, A. B. Heimberger, *Clin. Cancer Res.* **2021**, *27*, 4325.